# RESULTS ON DUST STORMS AND STATIONARY WAVES IN THREE MARS YEARS OF DATA ASSIMILATION.

**L. Montabone,** *Dept. of Physics - AOPP, University of Oxford, Oxford, UK - now at Laboratoire de Météorologie Dynamique du CNRS, Paris, France (montabone@lmd.jussieu.fr)*, **S. R. Lewis,** *Dept. of Physics & Astronomy, CEPSAR, The Open University, UK*, **P. L. Read,** *Dept. of Physics - AOPP, University of Oxford, Oxford, UK*.

## Introduction

Data assimilation is a technique which provides a complete, balanced, four-dimensional best-fit to observations for all the atmospheric variables, including those for which no direct measurements are available, such as wind and surface pressure. It represents, therefore, a unique opportunity to study both the inter-annual variability of the dust cycle and the behaviour of waves in the atmosphere of Mars. The access to information on surface wind stress, for instance, allows us to correlate dust storms and meteorology, and the global spatial and temporal coverage gives enough resolution to extract the properties of either stationary, transient or thermal tide waves (Lewis and Barker, 2005), which are difficult to study with measurements from a single sun-synchronous satellite.

We assimilated almost three complete Martian years of atmospheric temperature profiles and total dust opacities below about 40 km altitude into a general circulation model of the atmosphere, the Oxford version of the AOPP/LMD Mars general circulation model (MGCM) (Forget et al., 1999). The assimilation scheme which we used is based on the sequential Analysis Correction scheme of Lorenc et al. (1991), adapted and tuned for Martian data assimilation (Lewis et al., 1997, 2006). The data were provided by the Thermal Emission Spectrometer (TES) in nadir mode during the Mars Global Surveyor spacecraft (MGS) mapping phase which began in April 1999 and is still ongoing (though not routinely with the TES instrument).

In this paper we give some examples of the results which we obtained with this technique. These results are related to two topics: 1) the study of the inter-annual variability of dust storms and the conditions which can trigger the onset of a planet-encircling dust storm such as that of year 2001, and 2) the stationary waves in the lower Martian atmosphere. The stationary wave analysis has also been used for the purpose of validation of the results of the assimilation while comparing to an independent and simultaneous source of observations, such as the temperature profiles retrieved from the radio occultation measurements made with the ultra-stable radio oscillator on board MGS (Hinson et al., 1999, 2001), and acquired during approximately the same period of time as the assimilated TES profiles.

## Inter-annual variability of dust storms

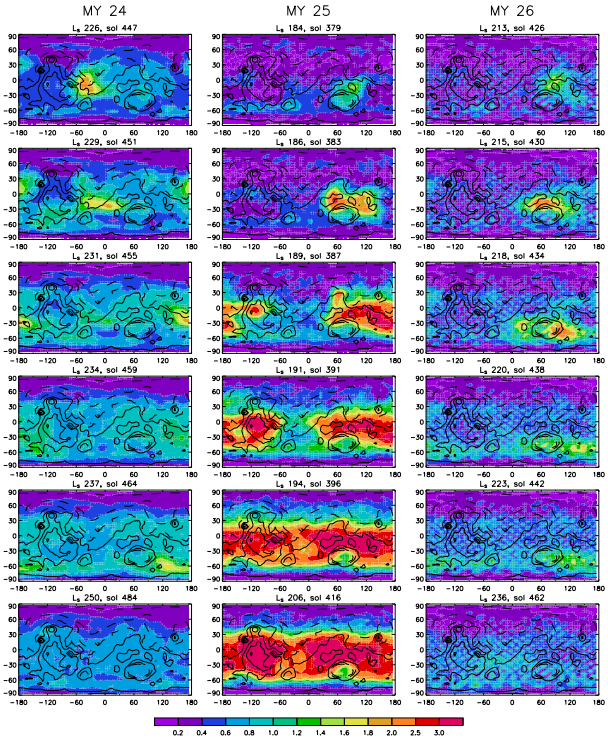


Figure 1: Evolution of dust storms in MY 24–26: distribution of the dust total optical depth normalized to 700 Pa

The overall variability of dust loading in the atmosphere over the three observed dust seasons appears to be quite large, although there are features with repeatable seasonal and spatial characteristics in all three Martian years (see Fig. 1 in Lewis et al., this issue). In particular, the picture highlights the extreme nature of the storm season in Martian Year (MY) 25 with respect to the other two, which corresponds to the planet-encircling dust storm of year 2001. The dust season in MY 25 shows both an increase in dust opacity of about three times more than the other seasons and an earlier and more rapid growth (see Fig. 1). The overall opacity starts to increase monotonically at $L_s \sim 185^\circ$ at a rate of about 0.14 per sol until $L_s \sim 195^\circ$ (on average, over a latitude band $40^\circ$N–$60^\circ$S. See also Fig. 2, upper panel), reaches its maximum at $L_s \sim 214^\circ$, then decreases more slowly over a range of more than 100 degrees of areo-

centric longitude. This global dust storm originated as a regional storm between Hellas and Isidis Planitia and rapidly grew to planetary scale thanks to the eastward migration and the consequent contribution of dust from the Tharsis region and the plains south of the Tharsis ridge. This could be due to a positive feedback within the dust cloud which serves to strengthen the near-surface wind stress, which in turn enhances the lifting of more dust (Newman et al., 2002). In MY 24 two regional dust storms developed in the Chryse region (at $L_s \sim 210^\circ$ and $L_s \sim 222^\circ$) and in the Amazonis region ($L_s \sim 226^\circ$), and faded out rapidly. MY 26 also exhibited a regional dust storm developing between Hellas and Isidis Planitia, although later than the previous year, but this did not grow sufficiently to produce a global storm, and faded out after only 12 sols. Nevertheless, a secondary peak of dust loading showed in this year around $L_s = 340^\circ$, corresponding to regional storms which contributed towards local warming of the lower atmosphere around the time of the landing of ESA's Beagle 2 and NASA's Mars Exploration Rovers.

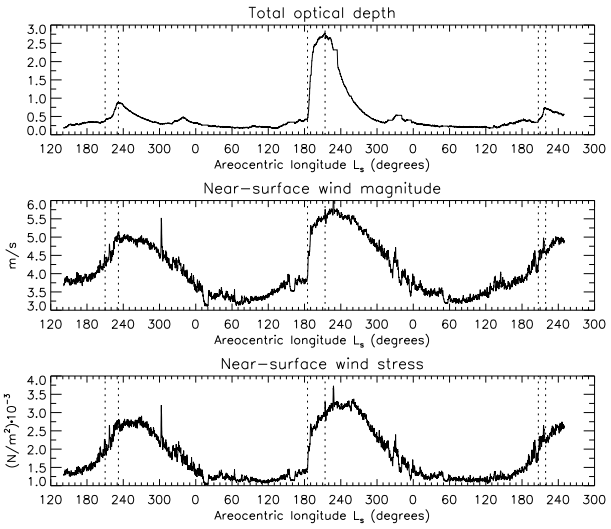


Figure 2: The upper panel represents the average of the dust optical depth at 700 Pa over the latitude band $40^\circ$N–$60^\circ$S, smoothed in time by using a 1-sol running mean. The middle panel is the average of the near-surface wind magnitude (wind speed at 4.6 m) over the same latitude band, and the lower panel is the average of the near-surface wind stress.

The onset and early development of dust storms are connected to the intensity of surface winds, which can be local or a manifestation of an enhanced global circulation. The variability of dust storm occurrence is determined mostly by the interannual variability of the local meteorology, enhanced or reduced by a number of positive or negative feedbacks which can originate from the the global circulation. Established dust storms, however, can have a big impact on the large scale variability. The possibility of dust devils (Rennó et al., 1998) triggering the onset of local dust storms should also be considered, since the amount of dust lifted by these atmospheric vortices can be considerable. Their strength, and therefore their ability to lift more dust, is determined by surface to air temperature difference and thermodynamic efficiency.

In order to characterize and try to explain the interannual variability of the onset of dust storms, we therefore analysed in the assimilation the variables which can be somehow related to the process of dust lifting, namely the near-surface wind stress (which depends on the wind speed), the surface to air temperature difference and the thermodynamic efficiency (Newman et al., 2002).

The interannual variability of near-surface winds and near-surface wind stress (at about 5m altitude) correlates very well in time with the variability of dust optical depth, as Fig. 2 shows. This picture plots the average of near-surface wind speed and wind stress over the latitude band $40^\circ$N–$60^\circ$S, smoothed by a 1-sol running mean, and compares them to the zonal mean of dust optical depth at 700 Pa averaged over the same latitude band. The comparison highlights that, on average, the dramatic increase in optical depth at $L_s \sim 185^\circ$ in MY 25 matches perfectly with the steep increase both in the magnitude of surface wind which, over 5 degrees of areocentric longitude (about 8 sols), becomes about 35% larger than in the other two years at the same time of year, and in the surface wind stress. Such an increase of surface wind magnitude with respect, for instance, to the previous year is at first concentrated around the northern and eastern slopes of Hellas basin (high slope winds), then extends to the Tharsis ridge, the Syria Planum and Solis Planum, south of Tharsis. According to the model of dust lifting described in Newman et al. (2002), this in turn should increase the amount of dust which is lifted in the air, although a preliminary study without transporting dust in the model was not able to reproduce the explosive increase of observed dust optical depth in MY 25 with respect to the increase in the previous year. Future work will address this issue in detail.

The effects of the planet-encircling dust storm are evident not only in the change of the dynamics of the atmosphere but also in the increase of the temperature below 60 km altitude, as shown in the upper panels in Fig. 3 for the period $L_s = 195^\circ$–$225^\circ$. The temperature increase during the global dust storm (right panels) is as large as $\sim 30$ K at a height of 20 km above the equator. This effect is due to the increased absorption of visible radiation by the suspended dust, which in turn has the consequence of cooling the surface by more than 20 K in some locations during the day. The combination of these two effects yields a negative feedback on the development of dust devils during dust storms, reducing the surface to air temperature difference, as described by Newman et al. (2002) and shown in Fig. 4, which is not compensated by any anomalous increase of ther-

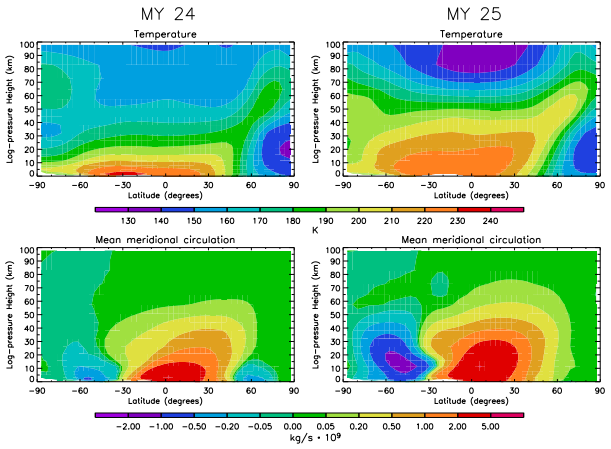


Figure 3: The plots show the temperature and mean meridional circulation averaged over 30 degrees of areocentric longitude ($L_s = 195^\circ - 225^\circ$) in two different years.

modynamic efficiency (see Fig. 5). The anticorrelation between these two variables suggests that the role played by convective vortices in lifting dust before and during the development of the global storm was marginal with respect to the lifting of dust by near-surface wind stress, which seems to be the prevalent mechanism for dust storm initiation.

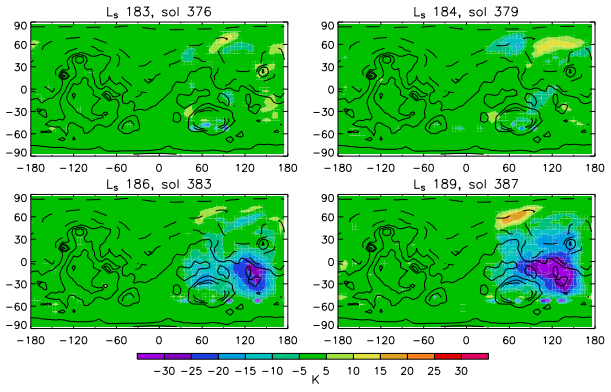


Figure 4: Difference between MY 25 and MY 24 of the surface to air temperature difference at noon at $90^\circ$E for four sols before and during the development of the dust storm around Hellas which leads to the global storm in MY 25.

## Stationary waves

Data assimilation with a general circulation model allows us to gain access not only to variables not directly assimilated, but also to full global coverage, both in space and time. The latter feature is essential for studying waves, transient and tidal in particular.

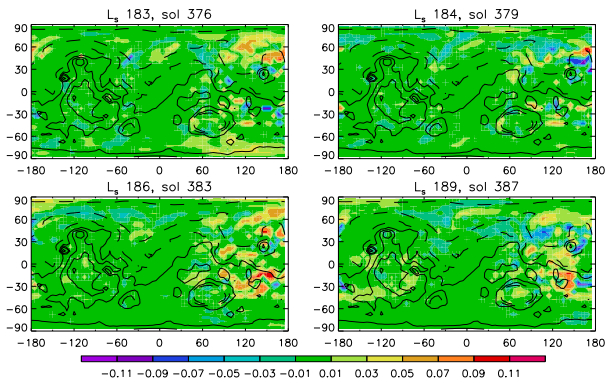


Figure 5: Same as in Fig. 4 for the thermodynamic efficiency

An important issue, nonetheless, is represented by the validation of the obtained results, ideally performed against an independent and simultaneous source of observations. We present here some results on waves which can be directly compared with observations. These are stationary waves which have also been measured by means of radio occultation soundings performed with the ultra-stable radio oscillator on board MGS.

A series of four direct comparisons between stationary waves obtained with assimilation and those obtained with radio occultation (Hinson et al., 2001, 2004) have been performed, namely for $L_s = 150^\circ$–$160^\circ$ at latitude 67°S in MY 24 and for $L_s = 52^\circ$–$58^\circ$ at latitude 62°N, $L_s = 76^\circ$–$82^\circ$ at latitude 65°N and $L_s = 99^\circ$–$109^\circ$ at latitude 75°N in MY 25. The comparison is made by using the stationary component of the temperature field, i.e. the average of temperature over the indicated period from which the zonal average has been subtracted. It is also possible to compare directly the wave-1 and wave-2 components of the field, obtained through a fourth-order decomposition at each pressure level $p$, $T'(\lambda, p) = \sum_{s=1}^{4} C_s(p) \cos[s\lambda - \gamma_s(p)]]$, where $C_s$ and $\gamma_s$ are the amplitude and phase, respectively, at zonal wavenumber $s$, and $\lambda$ is the longitude. Figure 6 shows an example of these quantities.

For the three last periods investigated, data assimilation shows a very good agreement with observations, although the MGCM does not resolve sharp vertical variations of temperature, as expected, such as those that appear in the first kilometers above the surface. For the first examined period, namely for the southern polar winter, however, the comparison highlights differences between the model and the observations which are known to be present during polar night. These differences might in part be related to problems of calibration for the TES observations, but are also certainly related to an incomplete representation of $CO_2$ processes (convection and formation of $CO_2$ clouds) during the Martian polar nights in the model. Work is in progress to improve these model parameterizations.

The latter result highlights another advantage of data

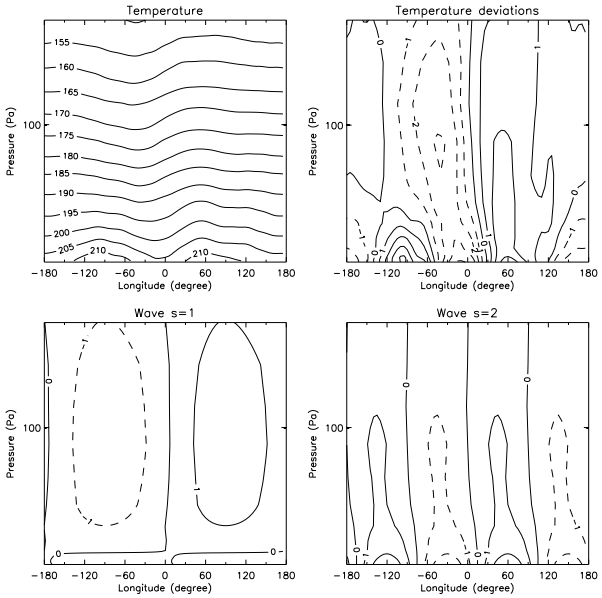


Figure 6: Temperature field, temperature deviation field, wave-1 and wave-2 components at latitude $62^\circ N$ and $L_s = 55^\circ$ in MY 25

assimilation, which can be used to test the model performance and to discover possible problems in a systematic way.

## Conclusions

In this paper we focused on some scientific results which were obtained by applying the data assimilation technique on Mars. These results on some aspects of the inter-annual variability of the dust storms and on the stationary waves show the capabilities of this technique, which is able to give access to global, 4-D information on all the atmospheric variables, even if the assimilated measurements are limited to a set of asynchronous temperature profiles and total dust opacities.

Further details about the topics discussed here can be found in Montabone et al. (2005a) and Montabone et al. (2005b)

## References

Forget, F., F. Hourdin, R. Fournier, C. Hourdin, O. Talagrand, M. Collins, S. R. Lewis, P. L. Read, J.-P. Hout, 1999. Improved general circulation models of the martian atmosphere from the surface to above 80 km. J. Geophys. Res. 104, 24,155–24,176.

Hinson, D. P., Simpson, R. A., Twicken, J. D., Tyler, G. L., 1999. Initial results from radio occultation measurements with mars global surveyor. J. Geophys. Res. 104 (E11), 26,997–27,012.

Hinson, D. P., Tyler, G. L., Hollingsworth, J. L., Wilson, R. J., 2001. Radio occultation measurements of forced atmospheric waves on mars. J. Geophys. Res. 106 (E1), 1463–1480.

Hinson, D. P.,M. D. Smith, B. J. Conrath, 2004. Comparison of atmospheric temperatures obtained through infrared sounding and radio occultation by Mars Global Surveyor. J. Geophys. Res. 109 (E12002).

Lewis, S. R., M. Collins and P. L. Read, 1997. Data assimilation with a Martian atmospheric GCM: An example using thermal data. Adv. Space Res. 19(8), 1267–1270.

Lewis, S. R., Barker, P., 2005. Atmospheric tides in a Mars general circulation model with assimilation of Mars Global Surveyor data. Adv. Space Res. 36(11), 2162–2168.

Lewis, S. R., P. L. Read, B. J. Conrath, J. C. Pearl and M. D. Smith, 2006. Assimilation of Thermal Emission Spectrometer atmospheric data during the Mars Global Surveyor aerobraking period. Submitted to Icarus.

Lorenc, A. C., Bell, R. S., Macpherson, B., 1991. The meteorological office analysis correction data assimilation scheme. Quart. J. R. Meteor. Soc. 117, 59–89.

Montabone, L., S. R. Lewis, P. L. Read, 2005a. Interannual variability of Martian dust storms in assimilation of several years of Mars Global Surveyor observations. Adv. Space Res. 36(11), 2146–2155.

Montabone, L., S. R. Lewis, P. L. Read, and D. P. Hinson, 2005b. Validation of Martian meteorological data assimilation for MGS/TES using radio occultation measurements. Icarus. Submitted.

Newman, C. E., S. R. Lewis, P. L. Read and F. Forget, 2002. Modeling the Martian dust cycle, 1. Representations of dust transport processes. J. Geophys. Res. 107(E12), 5123, doi:10.1029/2002JE001910.

Newman, C. E. and P. L. Read and S. R. Lewis, 2004. Investigating atmospheric predictability on Mars using breeding vectors in a gen eral circulation model. Q. J. R. Meteorol. Soc. , 130(603), 2971–2989.

Rennó, N. O., M. L. Burkett and M. P. Larkin, 1998. A simple thermodynamical theory for dust devils. J. Atmos. Sci., 55, 3244–3252.